MIT Open Access Articles

Modeling CO[subscript 2] Chemical Effects on CO Formation in Oxy-Fuel Diffusion Flames Using Detailed, Quasi-Global, and Global Reaction Mechanisms

Massachusetts Institute of Technology

Modeling CO_2 Chemical Effects on CO Formation in Oxy-Fuel Diffusion Flames using Detailed, Quasi-Global and Global Reaction Mechanisms

Lei Chen and Ahmed F. Ghoniem*

Department of Mechanical Engineering, Massachusetts Institute of Technology, 77 Massachusetts

Avenue, Cambridge, Massachusetts 02139-4307, United States

leichen@mit.edu, ghoniem@mit.edu

Corresponding author. Tel.: +1 617 253 2295; fax: +1 617 253 5981.

Abstract

Interest in oxy-fuel combustion as one of the leading carbon capture technologies has grown

significantly in the past two decades. Experimental studies have shown higher CO concentration in

oxy-fuel diffusion flames than in traditional air-fuel flames of both gaseous and solid fuels. The higher

CO concentration changes the flame profiles, and it may have impacts on pollutants formation. This

paper presents a numerical study regarding the chemical effects of CO_2 on CO formation in the flame

region, and their modeling approaches in CFD simulations. Equilibrium calculation confirms higher

CO concentration associated with fuel-rich stoichiometry in CO_2 diluted combustion environment.

One-dimensional counter flow diffusion flame simulation using detailed reaction mechanisms reveals

that the reaction $H+CO_2 \rightleftharpoons OH+CO$ enhances CO formation in the presence of high CO_2 concentration, leading to a significantly higher CO concentration under oxy-fuel combustion conditions. High CO_2 concentration also impacts the reaction $OH+H_2 \rightleftharpoons H+H_2O$ via OH radical and results in lower H_2 and higher H_2O concentrations in the flame profile. Computational Fluid Dynamics (CFD) simulations of a swirling diffusion flame under air-fired and oxy-fuel conditions were conducted using the Eddy Dissipation model and the Eddy Dissipation Concept model with quasi-global and global kinetic mechanisms. Results show that reasonable CO predictions can only be obtained using finite-rate approach with appropriate mechanisms considering the CO_2 chemical effects. The Westbrook-Dryer two-step mechanism consistently underestimates the CO concentrations. In contrast, the Westbrook-Dryer multiple-step mechanism captures the chemical effects of CO_2, and improves the predictions.

1. Introduction

Oxy-fuel combustion, often conducted using a mixture of oxygen and wet or dry recycled carbon dioxide, has attracted growing interest as one of the leading carbon capture technologies in power generation. The high CO_2 partial pressure in the oxidizing stream affects the thermodynamic, transport and chemical properties of the reacting medium, resulting in new characteristics in terms of the combustion temperature, heat transfer, reaction pathways, flame structure and pollutant formations (Buhre, Elliott, Sheng, Gupta and Wall 2005, Chen, Yong and

Ghoniem 2012, Toftegaard, Brix, Jensen, Glarborg and Jensen 2010, Wall, Liu, Spero, Elliott, Khare, Rathnam, Zeenathal, Moghtaderi, Buhre, Sheng, Gupta, Yamada, Makino and Yu 2009, Zheng 2011). For instance, the chemical effect of CO_2 has been shown to reduce the laminar burning velocity (Liu, Guo and Smallwood 2003, Zhu, Egolfopoulos and Law 1989) and produce higher CO concentration under premixed oxy-fuel combustions (Glarborg and Bentzen 2008) and diffusion oxy-fuel flames (Liu, Guo, Smallwood and Gülder 2001).

This study is most interested in the higher CO concentration in flame region which has been reported in oxy-fuel combustion tests, as compared to conventional air-fired combustion. For instance, increased CO level within the diffusion flame zone was reported in the experimental study performed in the IFRF 2.5 MW_{th} furnace by Woycenko et al. (Woycenko, van de Kamp and Roberts 1995). Likewise, Rehfeldt et al. (Rehfeldt, Kuhr, Ehmann, Bergins, Scheffknecht, Maier and Wu 2009) found significantly higher CO concentration in the fuel-rich flame region of oxy-Lausitz lignite coal combustion using a 0.5 MW_{th} pilot scale test facility. Moreover, Andersson et al. (Andersson, Johansson, Johnsson and Leckner 2008, Andersson and Johnsson 2007) and Hjartstam et al. (Hjartstam, Andersson, Johnsson and Leckner 2009) measured the CO concentrations in a 100 kW_{th} test facility using propane or lignite coal fuels, and they observed consistently higher CO concentrations in the combustion zone near the burner under oxy-fuel conditions than under air-fired conditions when the combustion temperatures are maintained the same. The higher CO in the flame region is expected to affect the pollutant formation processes. For instance, lower fuel-bound nitrogen conversions in oxy-fuel combustion were reported in the studies by Okazaki and Ando (Okazaki and Ando 1997) and Liu et al. (Liu, Zailani and Gibbs

2005), at least partially due to the higher CO concentration. The higher CO concentration in and around the boundary layer of the char particle in oxy-fuel combustion may also lead to a reduction in the amount of mineral suboxides and NO formed during oxy-char combustion (Chen, Yong and Ghoniem 2012).

The mechanism responsible for the higher CO concentration observed in the diffusion flames is still under investigation. It has been widely accepted that the different CO level is due to the CO_2 chemical effects in homogeneous and/or heterogeneous reactions (Chen, Yong and Ghoniem 2012, Toftegaard, Brix, Jensen, Glarborg and Jensen 2010), because CO_2 is not inert but it participates in the chemical reactions (Liu, Guo and Smallwood 2003, Liu, Guo, Smallwood and Gülder 2001, Masri, Dibble and Barlow 1992). However, it was not clear if the higher CO concentration is produced through CO_2 dissociation, i.e., $CO_2 \rightleftharpoons CO + 0.5O_2$, or through elementary reactions between CO_2 and intermediate species. Researchers have investigated both diffusion flames with CO_2 addition, and premixed oxy-combustion. Liu et al. (Liu, Guo, Smallwood and Gülder 2001) modeled the ethylene diffusion flame using a detailed mechanism, and CO_2 was added in the fuel side or oxidizer side with a mole fraction of 20%. The simulation showed higher CO concentrations with CO_2 addition in both sides, while introducing CO_2 on the oxidizer side has a more significant chemical effect than on the fuel side. Glarborg and Bentzen (Glarborg and Bentzen 2008) measured the CO concentration from highly diluted methane (~0.1%) premixed combustion at the exit of a plug-flow reactor in N_2 or CO_2 bulk gases under different equivalence ratios. Substantially higher CO concentrations were observed in the case of CO_2 dilution compared to those with N_2 dilution, in particular under

4

fuel-rich conditions. Simulation work in both studies identified the CO_2/H and CO_2/hydrocarbon fragment reactions as the major pathways responsible for the higher CO concentration. In oxy-coal combustion, the char-CO_2 and char-H_2O gasification reactions may also contribute to the higher CO in the fuel-rich region of the diffusion flame where oxygen concentration is low and the temperature is high. This heterogeneous pathway is not discussed in the present study, and the reader is referred to other relevant studies (Chen and Ghoniem 2012, Singer, Chen and Ghoniem 2012).

Secondly, appropriate modeling of the CO_2's chemical effects in computational fluid dynamics (CFD) simulations is required in order to get an accurate prediction of the CO formation in oxy-fuel combustion. The widely-used global reaction mechanisms used in CFD simulation were developed for traditional air-fired combustion, and they should be used with caution in oxy-fuel combustion because they may not capture the chemical effects of CO_2 in a high CO_2 concentration environment. Andersen et al. (Andersen, Rasmussen, Giselsson and Glarborg 2009) reviewed two global combustion mechanisms, namely the Westbrook and Dryer two-step mechanism (WD2) and Jones and Lindstedt four-step mechanism (JL4), and modified the kinetic parameters by calibrating the peak and equilibrium CO predictions in a plug flow reactor using a detailed mechanism under oxy-fuel conditions. The modified global mechanism improved the CO predictions, but there are still discrepancies between the measurements and simulations. More recently, Hjärtstam et al. (Hjärtstam, Normann, Andersson and Johnsson 2012) conducted a comparison study on the performance of several global mechanisms combing Eddy Dissipation Concept (EDC) model for oxy-fuel combustion modeling, and showed that the choice of reaction

5

mechanism strongly influence the prediction results, in particular the temperature, species and reaction rates.

The objective of this study is to further investigate the mechanisms responsible for the higher CO concentrations in oxy-fuel diffusion flames, and the appropriate approaches to model them in CFD simulations. The scopes of the paper are as follows:

- Confirm the CO_2 chemical effects on equilibrium CO concentrations under rich/lean conditions using thermodynamic calculation, and identify the operating conditions in which higher CO concentration is expected;

- Examine the critical reaction path for CO formation in air-fired and oxy-fuel diffusion flames; and

- Test and compare the performance of different gas phase reaction models and reaction mechanisms in CFD simulations.

Figure 1 shows the schematics of the one-dimensional laminar diffusion flame and the swirling flow turbulent diffusion flame under both air-fired and oxy-fuel conditions investigated in this paper. The performances of the detailed, quasi-global, and global mechanisms are compared, and their advantages and limitations in predicting the overall flame structure and CO concentration are further discussed.

2. Experiments

Many oxy-fuel combustion tests have been carried out in pilot scales since 1980s, however, available experimental measurements of CO concentration in the flame region with detailed

burner geometry and operating conditions are scarce. Therefore, available experimental results for air-fuel and oxy-fuel combustion are used in this study in order to test the performance of the combustion models and reaction mechanisms.

Andersson and coworkers (Andersson, Johansson, Johnsson and Leckner 2008, Andersson and Johnsson 2007) conducted an excellent work investigating propane flames under both air-fired and oxy-fuel combustion conditions using the Chalmers'100 kW_{th} test unit. Comprehensive temperature and gas composition measurements were carried out at different locations downstream of the burner. The test furnace consists of a swirl burner, a cylindrical refractory-lined furnace with an inner height of 2.4 m and an inner diameter of 0.8 m, a fabric filter, as well as a flue gas recycle system. Figure 1(b) shows a schematic of the swirl burner in the test facility: the burner consists of a fuel lance (i.d.=34 mm), surrounded by cylindrical primary and secondary feed-gas registers. The primary register is equipped with 45° swirl vanes and with an outer diameter of 52 mm, whereas the secondary register has a more moderate swirl number with a fin angle of 15° and outer diameter of 92 mm. In the air-fired case, air is used in the primary and secondary streams; while in the oxy-fuel cases, two different flue gas recycle rates (hence different oxygen fractions in the feed gas) were used. The oxygen mole fraction was 21% and 27% in the primary and secondary stream under the cases labeled OF21 and OF27, respectively, balanced by recycled dry flue gas consisting of mainly CO_2. In this study, we calculated the air-fired case and the OF27 case for their similar combustion temperatures and flame characteristics, and the stoichiometry was kept constant at stoichiometry of $\lambda = 1.15$.

Details of the gas compositions and mass flow rates under the air-fired and oxy-fuel operating conditions are summarized in Table 1.

3. Modeling Approaches

3.1. Thermodynamic Equilibrium Calculation

The species concentrations were calculated under thermodynamic equilibrium in $CH_4/O_2/N_2$ and $CH_4/O_2/CO_2$ systems using the Equilibrium model in CHEMKIN 4.0.

3.2. Modeling of the One-Dimensional Counter-Flow Diffusion Flame

The counter flow diffusion flame is modeled using the one-dimensional opposed-flow diffusion flame model in CHEMKIN 4.0. The fuel (methane) and oxidizer streams (either O_2/N_2 or O_2/CO_2) are injected from two concentric, circular nozzles directed towards each other, as shown in Figure 1(a). Mass, momentum and energy equations in the axisymmetric coordinate are solved using the stead state solver TWOPNT.

3.3. CFD Modeling of the Swirling-Flow Diffusion Flames

FLUENT 12.1 (ANSYS 2009) was used for the CFD simulations. A three-dimensional mesh with 400,000 hexahedral cells was used for the simulations of the Chalmers swirling flow diffusion flame. The mesh independence was checked by comparing the cold and reacting flow results using a double-sized mesh with 1,000,000 cells. The 400,000-cell mesh with 1 mm resolution in the burner region showed satisfactory accuracy at moderate computational cost.

The SST $k - \omega$ model (Menter 1994) was used for the swirling flow turbulence modeling because of its better performance in swirling flows based on our previous studies (Chen and Ghoniem 2012). The Discrete Ordinates (DO) model (Chui and Raithby 1993, Raithby and Chui 1990) was used to solve the radiative transfer equation (RTE) for radiative heat transfer, and the absorption coefficient of the participating gas mixture was modeled using weighted-sum-of-gray-gas model (WSGGM) (Hottel and Sarofim 1967) with modified parameters for oxy-fuel combustion as proposed by Johansson et al. (Johansson, Andersson, Leckner and Thunman). The modified WSGGM was implemented in the CFD simulation in the form of user defined functions (UDFs) as discussed in our previous validation study (Chen and Ghoniem 2012). Soot formation was observed to play a significant role in radiative heat transfer in the Chalmers experiments (Andersson and Johnsson 2007, Hjärtstam, Johansson, Andersson and Johnsson 2012). Therefore, soot formation was modeled using a one-step model (Khan and Greeves 1974), and the effect of the soot particles on the radiative heat transfer is considered by modeling its absorption coefficient in the RTE.

Two gas-phase reaction models, namely the eddy dissipation model (EDM) and eddy dissipation concept (EDC) model, were used in this study to model the turbulence-chemistry interaction. In the EDM (Magnussen and Hjertager 1977, Spalding 1971), the chemical reaction is governed by the large-eddy mixing time scale, defined as turbulence kinetic energy over its dissipation rate (k/ε), proposed by Spalding (Spalding 1971). Hydrocarbon combustion is assumed to take place in two irreversible steps:

$$C_nH_m + \left(\frac{2n+m}{4}\right)O_2 \rightarrow nCO + \frac{m}{2}H_2O \qquad (1)$$

$$CO + 0.5O_2 \rightarrow CO_2 \qquad\qquad\qquad (2)$$
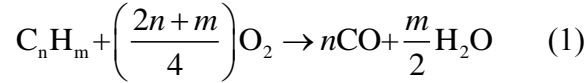
The EDM does not incorporate finite-rate kinetics, and the simplified gas phase reaction scheme in Equation (1)-(2) does not reflect the chemical effect of CO_2 on hydrocarbon oxidation discussed previously. Therefore, without tuning of its model parameters and validation work, this model can only be used to predict the major products species in stable diffusion flames in which the reaction rates are controlled by turbulent mixing, but is not expected to show accurate prediction of intermediate species such as CO and H_2 in oxy-fuel combustion. This will be discussed in more details later.

In the EDC model (Magnussen 1981, Magnussen and Hjertager 1977), the reactions are assumed to occur in small turbulent structures, or fine scales associated with the length fraction as a function of the average turbulence intensity. The EDC model can incorporate detailed chemical mechanisms, and it is possible to predict intermediate species, such as CO and H_2, given that appropriate reaction mechanisms are used. For global reaction mechanisms where the rate exponents are different from the stoichiometric coefficients, the backward reaction rate is computed using individual kinetic parameter sets which are obtained by calculating the backward reaction constant at a series of temperatures to guarantee chemical equilibrium.

3.4. Reaction Mechanisms

Table 2 summarizes the mechanisms that were tested in this numerical study, including detailed, quasi-global, and global mechanisms. Detailed reaction mechanisms for hydrocarbon combustion, such as the detailed chemical kinetic model (DCKM) presented by Glarborg and Bentzen (Glarborg and Bentzen 2008) and the GRI-Mech 3.0 used in our previous work (Chen, Yong and Ghoniem 2012), have been shown to be valid under oxy-fuel combustion conditions. Therefore, GRI-Mech 3.0 (Gregory P. Smith, David M. Golden, Michael Frenklach, Nigel W. Moriarty, Boris Eiteneer, Mikhail Goldenberg, C. Thomas Bowman, Ronald K. Hanson, Soonho Song, William C. Gardiner, Vitali V. Lissianski and Qin 2009) consisting of 53 species and 325 elementary reactions for CH_4 combustion was used in the one-dimensional counter flow diffusion flame modeling, and serve as benchmarks in the simulation.
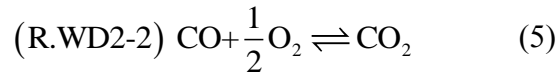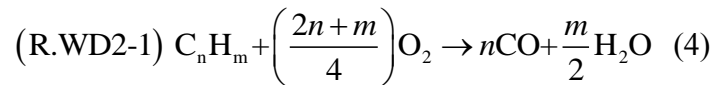
However, it is computationally expensive to apply detailed reaction mechanisms in CFD modeling. Alternatively, quasi-global or global hydrocarbon combustion mechanisms have been proposed. Westbrook and Dryer (Westbrook and Dryer 1984, Westbrook and Dryer 1981) proposed several simplified reaction mechanisms for the oxidation of hydrocarbon fuels in premixed flames, namely the WD one-step (WD1), WD two-step (WD2) and WD multi-step (WDmult) mechanisms. Later on, based on the analysis of premixed and diffusion flame structures, Jones and Lindstedt (Jones and Lindstedt 1988) proposed a four-step global reaction scheme (JL4) for hydrocarbon combustion. The features and limitations of these global and quasi-global mechanisms are as follows:

- **WD1** contains one-step global hydrocarbon oxidation reaction

$$(\text{R.WD1-1}) \ C_nH_m + \left(n + \frac{m}{4}\right)O_2 \rightarrow nCO_2 + \frac{m}{2}H_2O \quad (3)$$
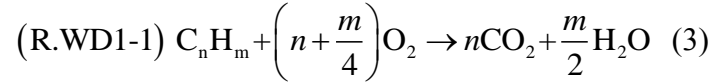
This global mechanism, with empirical kinetic parameters for different hydrocarbons, agrees well with the laminar burning velocity over a range of equivalence ratio However, it cannot predict CO or H_2.

- **WD2** contains two-step global reactions:

$$(\text{R.WD2-1}) \ C_nH_m + \left(\frac{2n + m}{4}\right)O_2 \rightarrow nCO + \frac{m}{2}H_2O \quad (4)$$

$$(\text{R.WD2-2}) \ CO + \frac{1}{2}O_2 \rightleftharpoons CO_2 \quad\quad (5)$$

This mechanism recognizes the fact that the hydrocarbons are first partially oxidized to CO before complete oxidation, and these two global reactions often proceed at different time scales. The reversible reaction (R.WD2-2) was proposed in order to reproduce the proper heat of reaction and the CO concentration at equilibrium, taking the form of CO_2 dissociation in a global manner. The rate of the CO oxidation was taken from Dryer and Glassman (Dryer and Glassman 1973), and (Westbrook and Dryer 1981). It should be noted that although the two-step reactions used in the EDM (in Equation (1)-(2)) has the similar form as the WD2 mechanism, those reactions in the EDM model are assumed to have infinite chemical kinetics and are irreversible.

- **WDmult** consists of an initiation reaction, in which CO and H_2 are produced in hydrocarbon partial oxidation, and 21 skeletal elementary reactions for CO-H_2-O_2 system. Therefore, it is a quasi-global mechanism. The initiation reaction is in the form of:

12

$$\left(\text{R.WDmult}-1\right)\ C_nH_m+\frac{n}{2}O_2 \rightarrow nCO+\frac{m}{2}H_2 \quad (6)$$
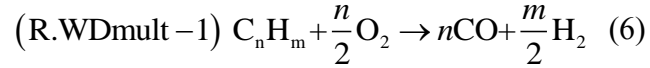
The CO-H_2-O_2 mechanism includes 11 species (H, O, H_2, O_2, OH, H_2O, N_2, CO, CO_2, HO_2 and H_2O_2) and 21 elementary reactions. The advantage of this mechanism is that it includes the critical elementary reactions in which CO_2 participates, hence no special treatments are required for the CO-H_2-O_2 system in a high CO_2 concentration environment.

Another global mechanism is the JL4 consisting of two initiation reactions, along with one reversible reaction for H_2 oxidation, and the reversible water gas shift reaction. The water gas shift reaction partially represents the CO_2 chemical effects in a global reaction manner, which may improve the CO concentration predictions. However, as has been discussed by Andersen et al (Andersen, Rasmussen, Giselsson and Glarborg 2009), a negative reaction order has to be assigned to H_2 for the reverse reaction in order to satisfy the equilibrium constant, hence numerical difficulties were encountered under fuel-lean conditions where hydrogen concentration approaches zero.

Based on the review of the reduced reaction mechanisms, the global mechanism WD2 and quasi-global mechanism WDmult were incorporated in the EDC model, because of their capability on predicting CO and their numerical robustness in commercial CFD software. The formulations and rates are summarized in Table 3. We note that the initiation reactions for methane and propane fuels are different and list them separately.

4. Results and Discussions

4.1. Thermodynamic Analysis of the CO Concentration in Oxy-Fuel Combustion

In a previous study, Zheng and Furimsky (Zheng and Furimsky 2003) calculated CO formation in coal combustion with O_2/N_2 and O_2/CO_2 at chemical equilibrium state. Under O_2/CO_2 condition, CO concentration was 316 ppm at 1700 K when burning with 10% excess oxygen, which was higher than that found in air combustion (64 ppm) at the same stoichiometry. The CO yield increases significantly to 0.201% at stoichiometry under O_2/CO_2 condition, comparing to 0.025% under O_2/N_2 condition. Even though, this difference is insignificant compared to that observed in the fuel-rich zone in the experiments (up to several percentage points) (Andersson and Johnsson 2007, Rehfeldt, Kuhr, Ehmann, Bergins, Scheffknecht, Maier and Wu 2009), indicating that the higher CO concentration in the oxy-fuel flame zone must be associated with specific stoichiometry.
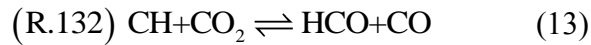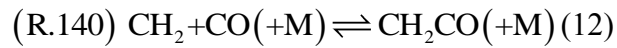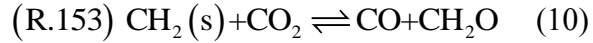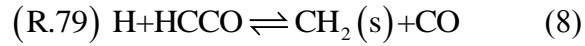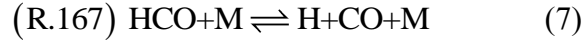
In this study, the equilibrium composition in methane/air and methane/(O_2+3.76CO_2) systems was calculated over a wider range of stoichiometry. Figure 2 shows the CO mole fraction as a function of gas temperature and stoichiometry at equilibrium. CO mole fraction increases with increasing the gas temperature and decreasing the stoichiometry under both air- and oxy-conditions, and the stoichiometry plays a significant role. When the stoichiometry, λ, is higher than unity, there is barely CO remaining in both cases due to complete burning. At $\lambda = 1.05$ which is a typical overall stoichiometry for combustion processes, the CO mole fraction difference between the air-fired and oxy-fuel environment is less than 1% up to 2000 K. However, under fuel-rich conditions, the difference increases drastically at high temperatures, showing that the CO_2 chemical effect is more prominent under fuel-rich conditions. The equilibrium CO mole fraction is up to 26% at 2000 K, significantly higher than the maximum

CO that can be produced through methane partial oxidation (~15%). Similar results have been reported in the experiment performed by Glarborg et al. (Glarborg and Bentzen 2008). We note that this operating condition only corresponds to the fuel-rich side of the diffusion flame. The equilibrium results cannot identify the pathway for the formation of CO, whether it is CO_2 dissociation under fuel-rich conditions, or CO_2 reduction, which will be investigated using detailed mechanism discussed in the following sub-section.

4.2. One-Dimensional Counter Flow Flames

The one-dimensional counter-flow diffusion flame structures under CH_4/Air and CH_4/O_2/CO_2 conditions were calculated using detailed mechanism GRI-Mech 3.0. The oxygen mole fraction in the oxy-fuel oxidizer jet was set to be 30% in order to maintain a similar peak combustion temperature (2002 K) as that of the air-fired case (2067 K). Figure 3 shows the predicted species mole fraction profiles. Under a strain rate of ~60 s^{-1}, the peak temperature is stabilized at about 1.12 and 1.02 cm away from the fuel nozzle outlet under air-fired and oxy-fuel conditions, respectively, indicating a slightly higher burning rate in the air-fired case. It can be seen that the CO concentration is significantly higher, and the H_2 concentration is slightly lower, in oxy-fuel flame than those in air-fuel flame.

An analysis on the CO production rates show that CO is mainly produced via two pathways in both cases. The first pathway is the reactions between intermediate hydrocarbon and active radicals, including (the reaction number before the formula is consistent with the consequence in GRI-Mech 3.0)

15

$$(\text{R.167}) \ \text{HCO+M} \rightleftharpoons \text{H+CO+M} \qquad (7)$$

$$(\text{R.79}) \ \text{H+HCCO} \rightleftharpoons \text{CH}_2(\text{s})\text{+CO} \qquad (8)$$

$$(\text{R.23}) \ \text{O+C}_2\text{H}_2 \rightleftharpoons \text{CO+CH}_2 \qquad (9)$$

$$(\text{R.153}) \ \text{CH}_2(\text{s})\text{+CO}_2 \rightleftharpoons \text{CO+CH}_2\text{O} \quad (10)$$

$$(\text{R.284}) \ \text{O+CH}_3 \rightleftharpoons \text{CO+H+H}_2 \qquad (11)$$

$$(\text{R.140}) \ \text{CH}_2\text{+CO}(\text{+M}) \rightleftharpoons \text{CH}_2\text{CO}(\text{+M}) \, (12)$$

$$(\text{R.132}) \ \text{CH+CO}_2 \rightleftharpoons \text{HCO+CO} \qquad (13)$$

We note that CO_2 participates in some of the above reactions directly, such as (R.153) and (R.132), or in the form of a third-body (M), such as (R.167), (R.140), which produces CO at high CO_2 concentration. The second pathway is the reaction between CO_2 and H radical

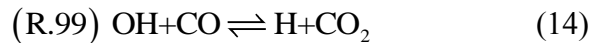$$(\text{R.99}) \ \text{OH+CO} \rightleftharpoons \text{H+CO}_2 \qquad (14)$$

Figure 4 compares the CO rate of production by these elementary reactions in air-fuel and oxy-fuel flames. The total CO production rate increases significantly from 0.5 kmol/m^{3}s in the air-fuel flame to 1.3 kmol/m^{3}s in the oxy-fuel flame, when the diluent changes from N_2 to CO_2. As discussed above, the higher total CO production rate in oxy-fuel flame are mainly attributed to hydrocarbon reactions in which CO_2 participates, such as (R.167), (R.153) and (R.132), and the backward reaction of the second pathway (R.99). Moreover, the second pathway reaction (R.99) dominates the CO production in the oxy-fuel flame, it contributes about one third of the

16

total CO in the fuel-rich side of the flame sheet. It also dominates the CO oxidation in the fuel-lean side of the flame under both air-fuel and oxy-fuel conditions.

Another interesting result in Figure 3 is the lower H_2 and higher H_2O concentrations in the oxy-fuel flame. Analysis shows that the elementary reaction

$$(R.84) \ OH+H_2 \rightleftharpoons H+H_2O \qquad (15)$$
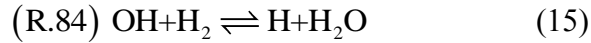
dominates H_2 production in the fuel-rich side, and H_2 oxidation in the fuel-lean side. In the fuel-rich side of the oxy-fuel flame, we have shown that the higher CO_2 concentration promotes the backward reaction of (R.99), which leads to a higher OH and lower H concentration in the radical pool. Consequently, the reaction (R.84) is pushed forward, and H_2 is shifted to produce H_2O. Figure 5 compares the H_2 rate of production due to (R.84), along with the CO rate of production due to (R.99), between the air-fuel and oxy-fuel flames. The results show that the backward reaction of (R.84) is inhibited in the oxy-fuel flame, which leads to lower H_2 production rate. Moreover, different from the air-fuel flame in which CO and H_2 are produced and consumed simultaneously in the fuel-rich and fuel-lean sides, there is a region between 1.00 and 1.02 cm in the flame sheet, where CO is produced through (R.99) and H_2 is consumed through (R.84). The combined effect of these two elementary reactions is the backward water gas shift reaction

$$CO+H_2O \rightleftharpoons CO_2+H_2 \qquad (16)$$
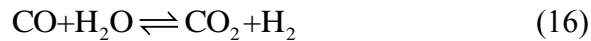
In a global reaction perspective, the higher CO_2 concentration moves the equilibrium of the water gas shift reaction, leading to lower H_2 but higher CO and H_2O concentrations in the fuel-rich side of the diffusion flame sheet.

The performances of the quasi-global mechanism WDmult and the global mechanism WD2 are tested and compared with the benchmark GRI-mech 3.0. Figure 6 shows the predicted CO mole fractions under CH_4-Air and CH_4-O_2/CO_2 conditions using these mechanisms. It is interesting to see that both quasi-global and global mechanisms perform reasonably and show the higher CO concentration trend in oxy-fuel combustion. In the WDmult mechanism, the critical elementary reactions responsible to the CO_2 chemical effects have been included, therefore, it can represent the higher CO trend in oxy-fuel combustion. While the WD2 mechanism models the CO concentration through the reversible reaction $\left(\text{R.WD2-2}\right) CO + \frac{1}{2}O_2 \rightleftharpoons CO_2$. At high temperature, both forward and backward reaction rates are high enough to ensure the chemical equilibrium, hence the higher CO concentration under oxy-fuel condition is predicted as well. Note that WD2 over predicts the CO at the fuel-lean side, because the kinetic parameters used in the global reaction are off the equilibrium at high CO2 conditions, and this will be discussed also in section **Error! Reference source not found.**.

In summary, the analysis has identified the reaction pathways in which higher CO_2 concentration influences CO formation in the oxy-fuel diffusion flames: it reacts with hydrocarbon fragments in the fuel-rich side, and promotes the $H + CO_2 \rightleftharpoons OH + CO$ reaction, resulting in a higher CO concentration. Interacting with the $OH + H_2 \rightleftharpoons H + H_2O$ reaction, higher CO_2 also leads to lower H_2 and higher H_2O concentration. This has implications regarding

18

the use of the reduced mechanisms. To capture the first pathway, appropriate kinetic parameters should be used for the initiation reaction, taking the chemical effect of CO_2 on hydrocarbon-CO_2 reactions into account. Regarding the second pathway, either critical elementary reactions, such as $H+CO_2 \rightleftharpoons OH+CO$ and $OH+H_2 \rightleftharpoons H+H_2O$, should be calculated directly as the WDmult mechanism does; or the CO/CO_2 equilibrium should be modeled using global reversible reactions as the WD2 mechanism or JL4 mechanism (see Ref. (Hjärtstam, Normann, Andersson and Johnsson 2012)) do. Although the reduced mechanism and global mechanism capture the CO trends in the relatively simple one-dimensional laminar diffusion flame, their performances for turbulent diffusion flames should be further investigated because of the turbulence-chemistry interactions and the multi-scale nature of the chemical reactions.

4.3. Swirling Flow Diffusion Flames

The swirling flow diffusion flame structure has been shown schematically in Figure 1(b). In swirl burner flow, reverse pressure gradient is generated along the axis forcing the hot gas to recirculate and mix with unburned streams in an internal recirculation zone (IRZ), which increases the flame intensity and stabilizes the diffusion flame. Therefore, it has been widely used in gaseous fuels and pulverized coal combustion (Beer and Chigier 1983). The internal recirculation zone features high temperature and fuel-rich stoichiometry, which is favorable for CO formation as discussed in the thermodynamic analysis. In this section, the predicted temperature and species distribution are compared with measurements in the Chalmers 100 kW_{th}

test facility. Special attention is given to the CO formation mechanism in the flame zone, and the performances of different combustion models and reaction mechanisms in such a case.

Figure 7 shows comparison between the measured and predicted gas temperature along the axis of the furnace under air-fired and oxy-fuel conditions. Satisfactory agreements are obtained with all approaches, except that the predicted gas temperatures are all slightly higher than the measurements, especially in the flame region, probably because of the fact that not all minor radicals were calculated in the species transport and energy equations. All the predictions show the temperature rise at the flame zone, which is stabilized near the swirl burner, and a similar declining temperature profile due to mixing and heat transfer downstream. It should be noted that the temperature profiles were significantly improved when the soot formation and its radiation were modeled in both air-fired and oxy-fuel combustion. Soot particles participate in radiation absorption and emission, make additional contribution to the absorption coefficient of the gas phase. Figure 8 shows the comparison of predicted temperature profile with and without using soot model, the peak temperature with considering soot radiation is reduced by 100-200 K than the simulation results without soot model. This has also been shown in previous study in ref. (Hjärtstam, Johansson, Andersson and Johnsson 2012).

Figure 9 shows a comparison between the measured and predicted oxygen mole fraction radial profiles at x=0.215 and x=0.384 m away from the burner. The EDM with two-step reaction mechanism (termed as "infinite-fast") shows generally good match with the measurements under both air-fired and oxy-fuel conditions, this indicates that the EDM is still valid to predict major species under oxy-fuel conditions. On the other hand, the finite-rate mechanisms also agree with

the measurement in the air-fired combustion, but slightly lower than those from the EDM, which translates to faster oxygen consumption rates. In the oxy-fuel combustion case, the WD2 mechanism over-predicts the oxygen mole fractions at 0.215 and 0.384 m away from the burner. As has been discussed previously in section 4.2, this again is due to the non-equilibrium backwards reaction rate (Andersen, Rasmussen, Giselsson and Glarborg 2009), whose effect is magnified by high CO_2 concentrations. While the WDmult mechanism shows much better match with the measurement.

The performances of EDM and EDC approaches with various reduced mechanisms on CO concentration predictions are apparently different. Figure 10 shows the measured and predicted CO radial profiles at x=0.215 and x=0.384 m. The EDM significantly underpredicts the CO concentrations in both air-fired and oxy-fuel combustion, and it failed to show the higher CO trend in oxy-fuel combustion because the reaction rates are assumed to be controlled by the turbulent mixing only, while the chemical kinetics are assumed to be infinitely fast. The WD2 mechanism improves the CO predictions and shows the higher CO trend in oxy-fuel combustion. However, it still underestimates the CO concentrations in both cases. Note that the WD2 mechanism cannot approach chemical equilibrium and leads to 1% and 3% residual CO (~1%) in the furnace under air-fired and oxy-fuel combustion, respectively, which agree well with the study by Andersen et al. (Andersen, Rasmussen, Giselsson and Glarborg 2009). In contrast, the WDmult mechanism significantly improves the CO predictions in both air-fired and oxy-fuel combustion, because it includes the critical reactions discussed in section 4.

21

We have shown in the one-dimensional diffusion flame calculation that the $H+CO_2 \rightleftharpoons OH+CO$ reaction dominates the higher CO production rate and leads to higher CO concentration in oxy-fuel combustion. This is captured by the EDC model with the WDmult mechanism in the CFD simulation. Figure 11(a) compares the CFD predicted CO and O_2 contour along with the velocity field in vicinity of the burner under the air-fired and oxy-fuel conditions. The vector flowfield shows that an IRZ is formed by the swirled primary and secondary oxidizer streams (air or O_2/CO_2), which stabilizes the flame in the vicinity of the burner. The combustion reactions take place mostly around the diffusion flame sheet between the fuel-rich zone and the oxidizer-rich streams. CO and other active radicals are produced in the fuel-rich side of the diffusion flame sheet, and recirculated back to the burner along with the burned hot gases. Figure 11(b) compares the reaction rate of $OH+CO \rightleftharpoons H+CO_2$ in the air-fuel and oxy-fuel flames. The significantly higher backward reaction rate of $OH+CO \rightleftharpoons H+CO_2$ in the oxy-fuel flame leads to its substantially higher CO concentration in the IRZ.

Figure 12 provides greater details about the predicted flame structures at 0.05 m away from the burner under the two operating conditions (the profile location is also illustrated in Figure 11). The species concentrations are uniform around the centerline due to the strong mixing in the IRZ. The species mole fraction profiles again indicate a diffusion flame sheet in the interface between the fuel-rich recirculation zone and the surrounding oxidizer streams. Note that higher CO and H_2O, and lower H_2 concentrations are observed in the recirculation zone under oxy-fuel condition. The backward reaction rate of $OH+CO \rightleftharpoons H+CO_2$ in the oxy-fuel flame sheet is

22

about 1 kmol/m^{3}s, significantly higher than that (almost 0) in the air-fuel flame, which explains the higher CO concentration in oxy-fuel combustion. Similar to the one-dimensional diffusion flame, the high CO_2 concentration also impacts the reaction $OH+H_2 \rightleftharpoons H+H_2O$, and results in lower H_2 in the oxy-fuel flame.

5. Conclusion

Higher CO concentrations have been observed in oxy-fuel combustion than the traditional air-fuel combustion by previous experimental studies. In this paper, the CO_2 chemical effects on CO formation have been investigated through thermodynamic analysis, one-dimensional simulation of the counter flow laminar diffusion flame using detailed mechanism, and three-dimensional CFD simulation of swirling flow turbulent diffusion flames using quasi-global and global reaction mechanisms . The main findings are as follows:

(1) From a thermodynamic point of view, significantly higher CO concentration observed in oxy-fuel flames is expected under fuel-rich conditions only, corresponding to the fuel-rich side of the oxy-fuel diffusion flame.

(2) CO formation is enhanced by the high CO_2 concentration through two reaction pathways under oxy-fuel condition: (a) the hydrocarbon fragment-CO_2 reactions and (b) the $OH+CO \rightleftharpoons H+CO_2$ reaction. The latter one dominates the CO formation, resulting in higher CO concentration, and it also interacts with the $OH+H_2 \rightleftharpoons H+H_2O$ reaction, leading to lower H_2 and higher H_2O in the reaction region. The combination effect of the above reactions may be

23

partially represented in the form of water gas shift reaction $CO+H_2O \rightleftharpoons CO_2+H_2$ in the fuel-rich side.

(3) EDM with infinite-fast chemistry can still be used to predict the temperature and major species in the swirling flow turbulent diffusion flame under both air-fired and oxy-fuel conditions, however it fails to predict CO concentration reasonably. Combining with EDC model, the WD2 global reaction mechanism models the CO_2 chemical effect through the CO_2 dissociation reaction and can capture the higher CO concentration trend in the one-dimensional diffusion flame. However, it consistently underestimates the CO concentrations in the CFD simulations. The WDmult quasi-global reaction mechanism contains critical elementary reactions, and it is able to capture the chemical effects of CO_2 in oxy-fuel combustion, showing improved performance in both air-fuel and oxy-fuel flame CFD simulations.

Acknowledgement

Tables

Table 1. The operating conditions of the propane combustion experiment under air-fired and oxy-fuel conditions.

Streams	Temperature °C	Mass flow rate (kg/s) and mole fraction (vol%) in $O_2:N_2:CO_2$	
		Air	OF27
Fuel lance	25	1.67e-3 (Propane)	1.67e-3 (Propane)
Primary stream	25	1.22e-2 (21:79:0)	1.33e-2 (27:2:71)
Secondary stream	25	1.78e-2 (21:79:0)	1.93e-2 (27:2:71)

Table 2. A summary of the mechanisms tested in this study.

Mechanism	Species	Reactions	Calculated Cases	Reference
GRI-mech 3.0	53	325	1-D counter flow diffusion flame	(Gregory P. Smith, David M. Golden, Michael Frenklach, Nigel W. Moriarty, Boris Eiteneer, Mikhail Goldenberg, C. Thomas Bowman, Ronald K. Hanson, Soonho Song, William C. Gardiner, Vitali V. Lissianski and Qin 2009)
WDmult	12	22	1-D counter flow diffusion flame, Swirling Flow diffusion flame	(Westbrook and Dryer 1984, Westbrook and Dryer 1981)
WD2	5	2	1-D counter flow diffusion flame, Swirling Flow diffusion flame	(Dryer and Glassman 1973, Westbrook and Dryer 1984, Westbrook and Dryer 1981)

Table 3. The quasi-global and global reaction mechanisms used for CH_4 and C_3H_8 combustion under air- and oxy-fuel conditions (Units are in m-sec-kmol-J-K).

Reaction No.	Reaction	A_r	E_r	β_r	Reaction orders
WD Multi-Step (Westbrook and Dryer 1984, Westbrook and Dryer 1981)					
WDmult-1	$CH_4 + 0.5O_2 \rightarrow CO + 2H_2$	7.54e11	2.00e8	0	$[CH_4]^{0.7}[O_2]^{0.8}$

	$C_3H_8 + 1.5O_2 \rightarrow 3CO + 4H_2$	3.38e10 (8.44e9)[a]	1.25e8	0	$[C_3H_8]^{0.1}[O_2]^{1.65}$
WDmult-2	$H + O_2 = O + OH$	2.20e11	7.02e7	0	
WDmult-3	$H_2 + O = H + OH$	1.80e7	3.72e7	1	
WDmult-4	$O + H_2O = OH + OH$	6.80e10	7.69e7	0	
WDmult-5	$OH + H_2 = H + H_2O$	2.20e10	2.13e7	0	
WDmult-6	$H + O_2 + M = HO_2 + M$	1.50e9	-4.18e6	0	
WDmult-7	$O + HO_2 = O_2 + OH$	5.00e10	4.18e6	0	
WDmult-8	$H + HO_2 = OH + OH$	2.50e11	7.94e6	0	
WDmult-9	$H + HO_2 = H_2 + O_2$	2.50e10	2.93e6	0	
WDmult-10	$OH + HO_2 = H_2O + O_2$	5.00e10	4.18e6	0	
WDmult-11	$HO_2 + HO_2 = H_2O_2 + O_2$	1.00e10	4.18e6	0	
WDmult-12	$H_2O_2 + M = OH + OH + M$	1.20e14	1.90e8	0	
WDmult-13	$HO_2 + H_2 = H_2O_2 + H$	7.30e8	7.82e7	0	
WDmult-14	$H_2O_2 + OH = H_2O + HO_2$	1.00e10	7.52e6	0	
WDmult-15	$CO + OH = CO_2 + H$	1.50e4	-3.34e6	1.3	
WDmult-16	$CO + O_2 = CO_2 + O$	3.10e8	1.57e8	0	
WDmult-17	$CO + O + M = CO_2 + M$	5.90e9	1.71e7	0	
WDmult-18	$CO + HO_2 = CO_2 + OH$	1.50e11	9.91e7	0	
WDmult-19	$OH + M = O + H + M$	8.00e16	4.34e8	-1	
WDmult-20	$O_2 + M = O + O + M$	5.10e12	4.81e8	0	

WDmult-21	$H_2+M=H+H+M$	2.20e11	4.01e8	0	
WDmult-22	$H_2O+M=H+OH+M$	2.20e13	4.39e8	0	

WD two-Step (Dryer and Glassman 1973, Westbrook and Dryer 1981)

WD2-1	$CH_4+1.5O_2 \rightarrow CO+2H_2O$	5.03e11	2.00e8	0	$[CH_4]^{0.7}[O_2]^{0.8}$
	$C_3H_8+3.5O_2 \rightarrow 3CO+4H_2O$	5.62e9	1.25e8	0	$[C_3H_8]^{0.1}[O_2]^{1.65}$
WD2-2f	$CO+0.5O_2 \rightarrow CO_2$	2.24e12	1.67e8	0	$[CO]^{1}[O_2]^{0.25}[H_2O]^{0.5}$
WD2-2r	$CO_2 \rightarrow CO+0.5O_2$	5.00e8	1.67e8	0	$[CO_2]^{1}$

[a] The global reactions parameters shown in brackets are for oxy-fuel combustion.

Figures
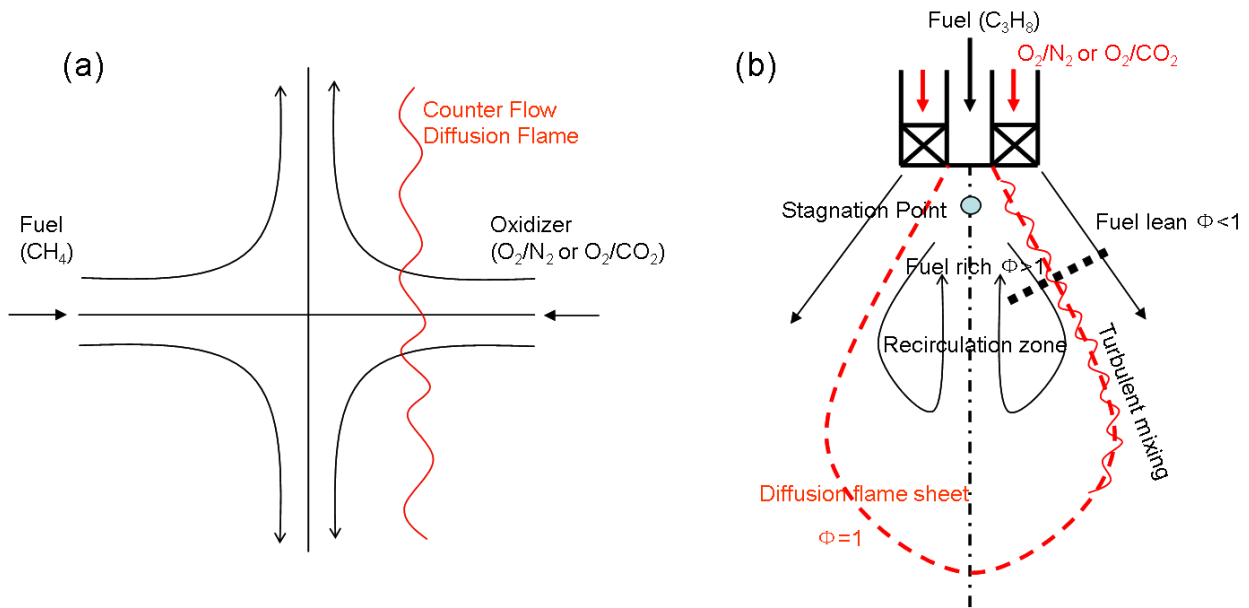
Figure 1. Schematic of two diffusion flames in the present study: (a) A counter flow laminar diffusion flame, and (b) a swirling flow turbulent diffusion flame.
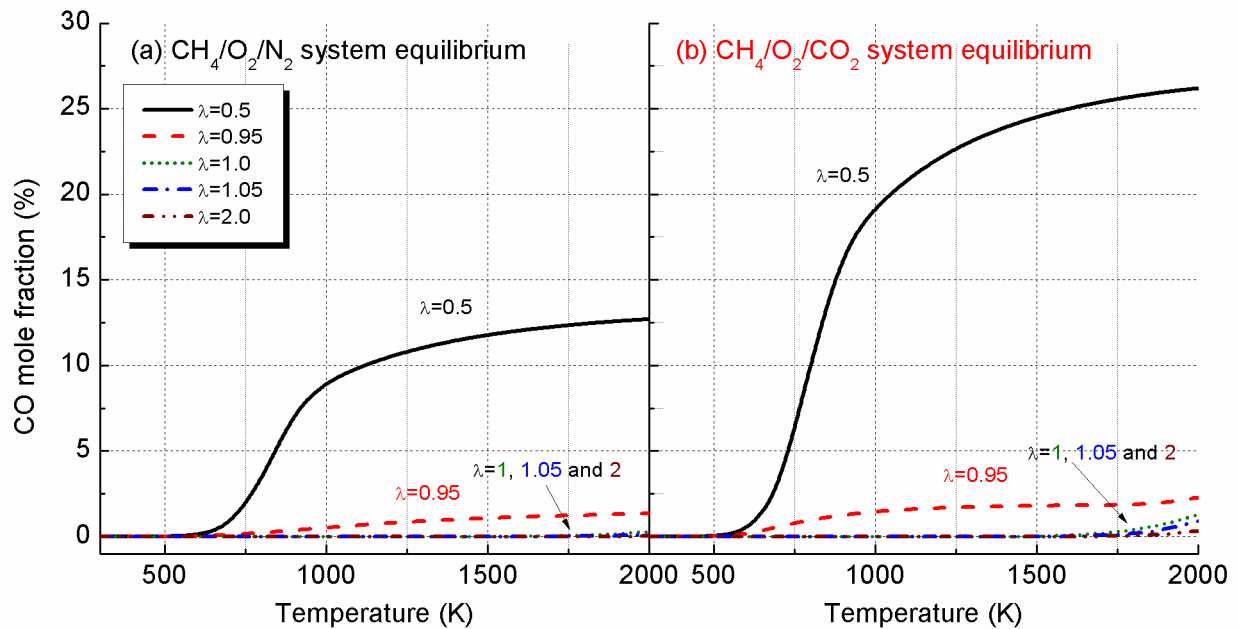
Figure 2. The CO mole fraction at thermodynamic equilibrium in $CH_4/O_2/N_2$ and $CH_4/O_2/CO_2$ systems as a function of temperature and stoichiometry.
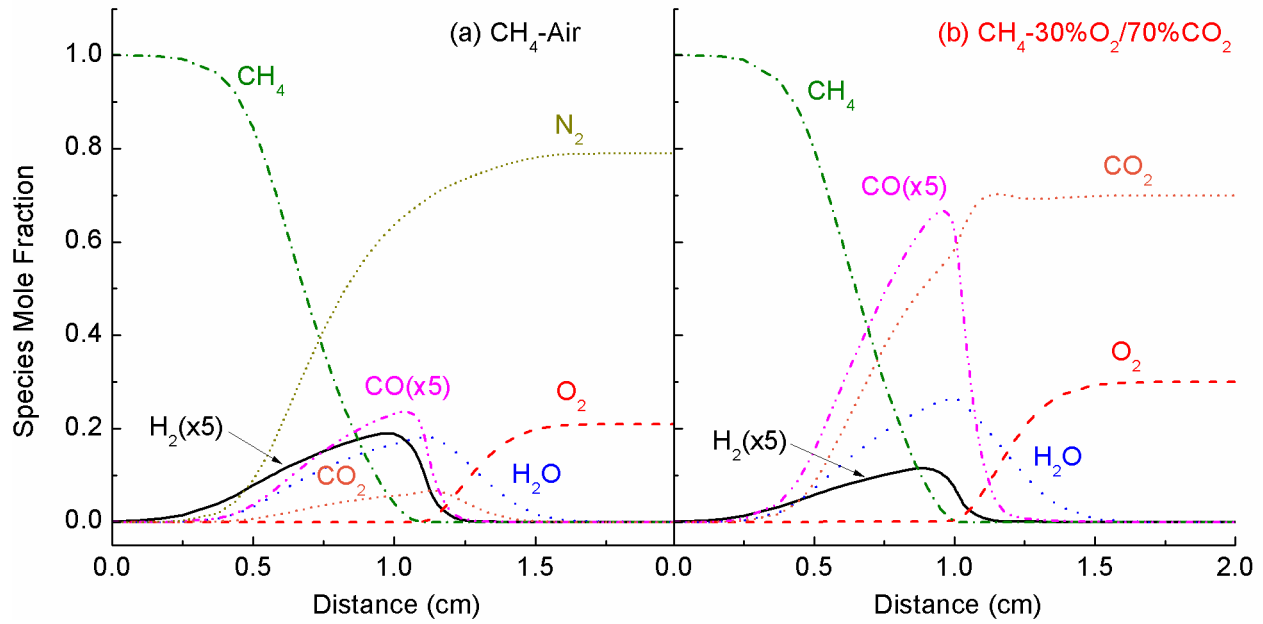
Figure 3. Counter flow diffusion flame structures in (a) air-fired and (b) oxy-fuel combustion under a strain rate of 60 s^{-1}. Results are predicted using GRI-Mech 3.0 detailed mechanism. Note that CO and H$_2$ mole fractions are enlarged 5 times in the figure.
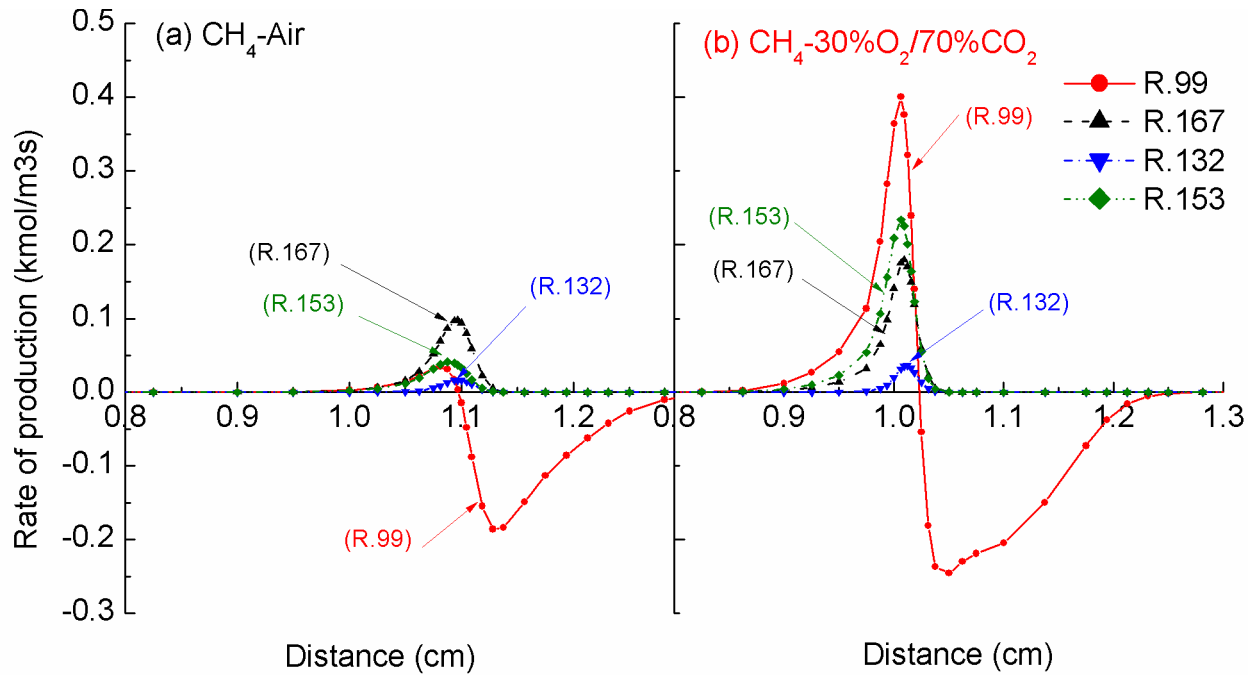
Figure 4. CO rate of production due to reactions (R.99), (R.167), (R.132), and (R.153) under (a) air-fired and (b) oxy-fuel conditions. Results are predicted using GRI-Mech 3.0 detailed mechanism, and the strain rate is 60 s^{-1}.
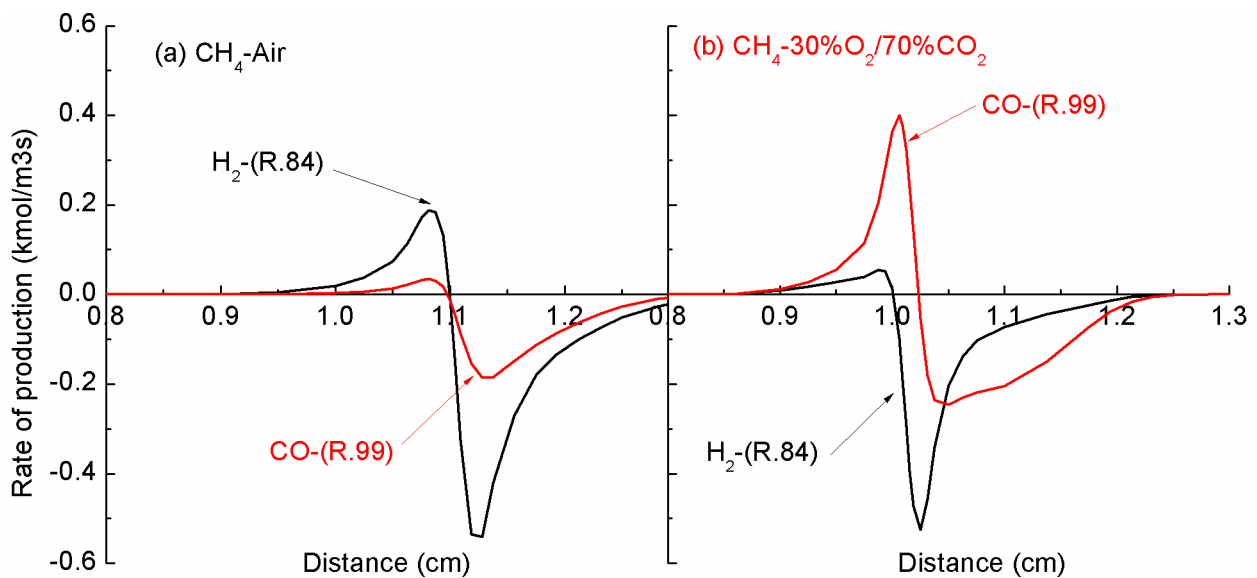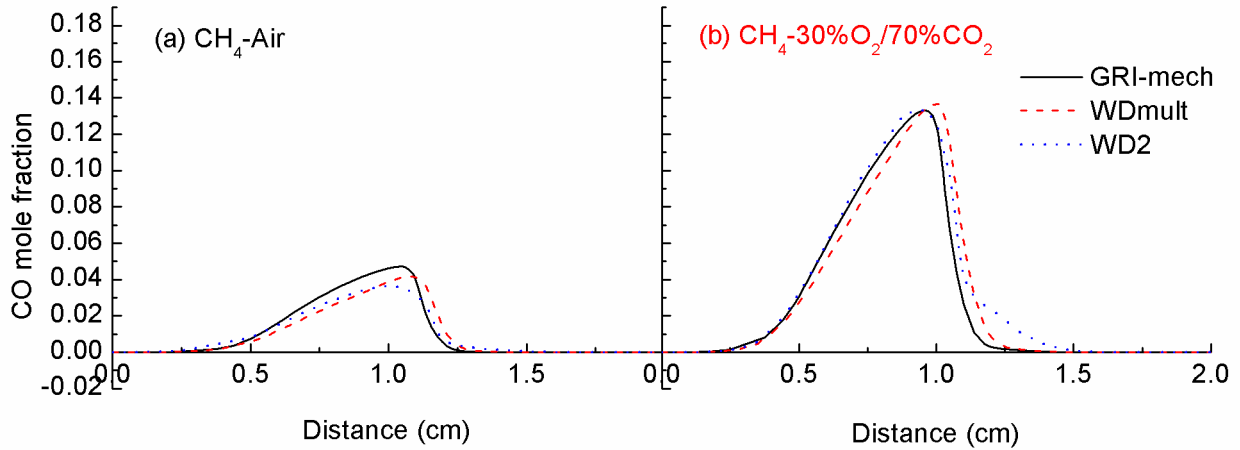

Figure 5. H$_2$ and CO rate of production due to reactions (R.84) and (R.99) under (a) air-fired and (b) oxy-fuel conditions. Results are predicted using GRI-Mech 3.0 detailed mechanism, and the strain rate is 60 s^{-1}.

Figure 6. Comparison of the predicted CO mole fractions in 1D counter flow diffusion flame using GRI-Mech 3.0, WDmult and WD2 mechanisms under (a) air-fired and (b) oxy-fuel conditions. The strain rate is 60 s^{-1}.
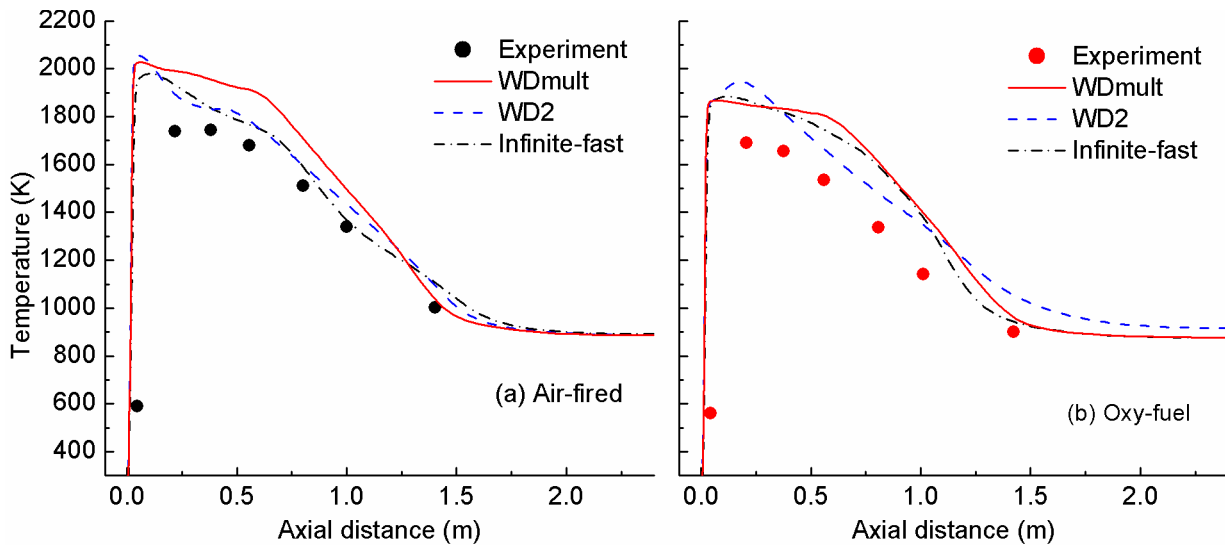

Figure 7. Comparison between the measured (scatters) and predicted (lines) axial temperature in (a) air-fired, and (b) oxy-fuel combustion. Simulation results were obtained using different gas phase reaction models and reaction mechanisms (Infinite-fast represents EDM with infinite-fast chemistry).
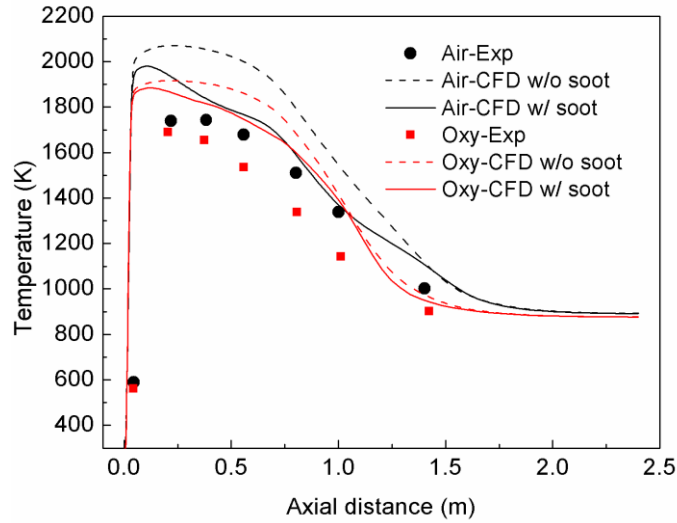
Figure 8. Comparison between the measured (scatters) and predicted (lines) axial temperature in air-fired and oxy-fuel combustion. Simulation results were obtained using EDM with or without soot model.　(a) Air-fired　　　　　　　　　　　　(b) Oxy-fuel
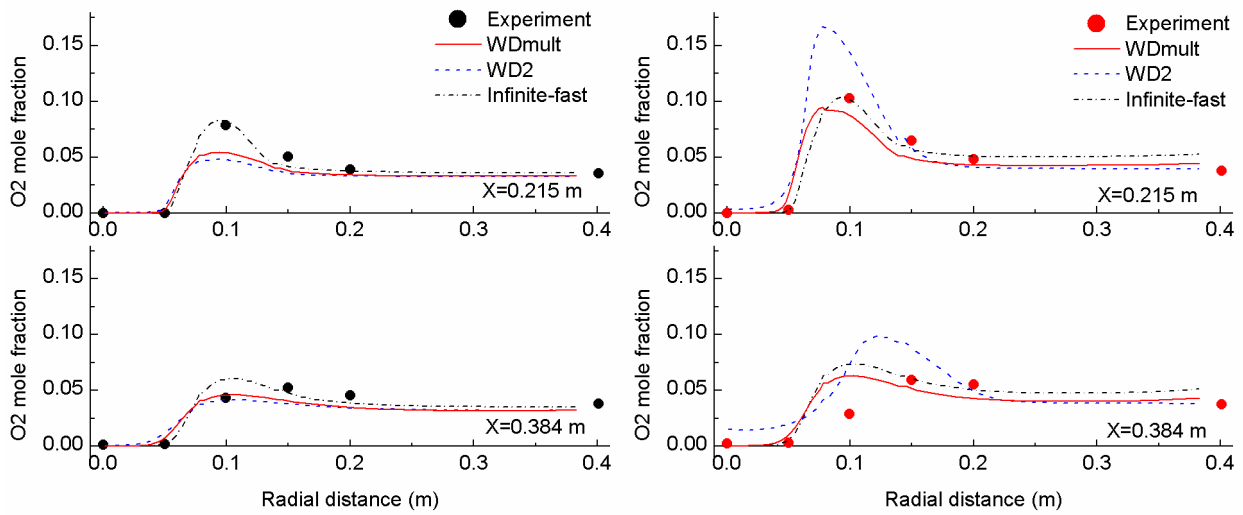

Figure 9. Comparison between the measured (scatters) and predicted (lines) oxygen mole fractions (dry basis) at 0.215 and 0.384 m away from the burner in (a) air-fired, and (b) oxy-fuel combustion.

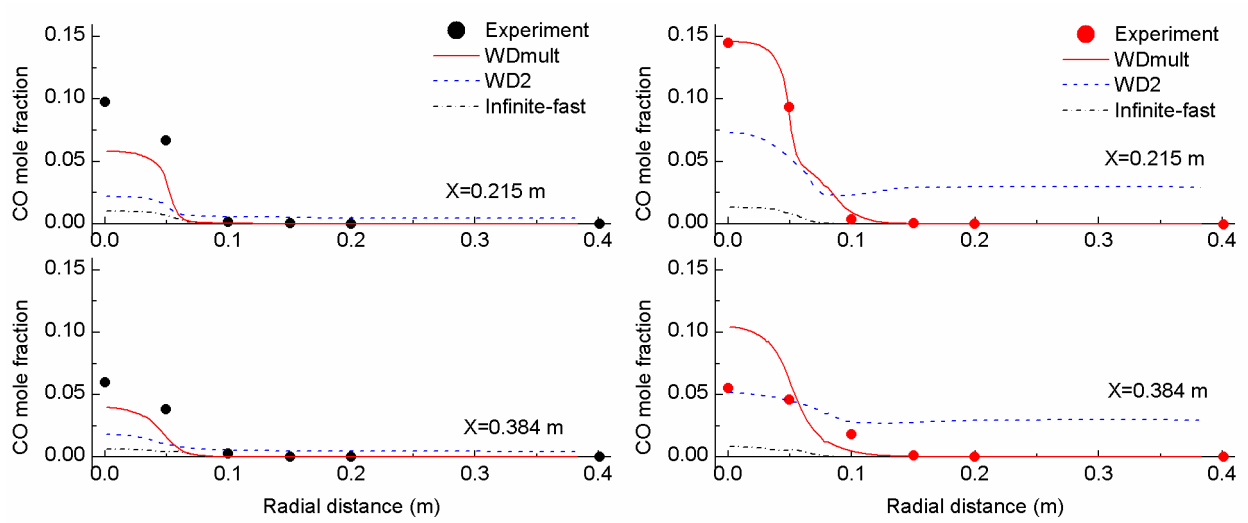(a) Air-fired   (b) Oxy-fuel

Figure 10. Comparison between the measured (scatters) and predicted (lines) CO mole fractions (dry basis) at 0.215 and 0.384 m away from the burner in (a) air-fired, and (b) oxy-fuel combustion.
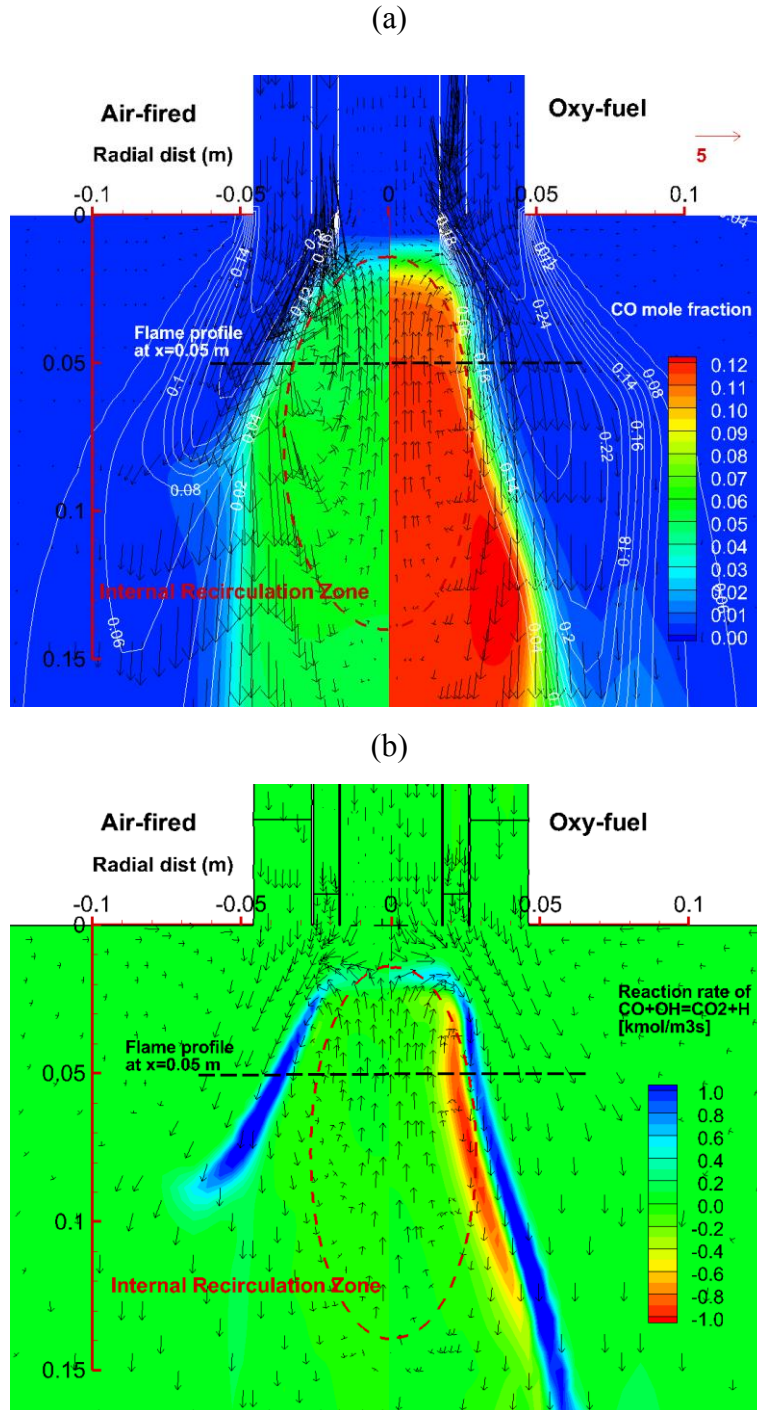
(a)

(b)

Figure 11. Comparison between air-fired (left) and oxy-fuel (right) combustion: (a) the oxygen mole fractions and the carbon monoxide mole fraction shown in isoline and color contour, respectively; and (b) the reaction rate of $OH+CO \rightleftharpoons H+CO_2$ shown in color contour in the vicinity of the swirl burner. The velocity field is shown using uniform vectors. Results are obtained using the WDmult reaction mechanism.
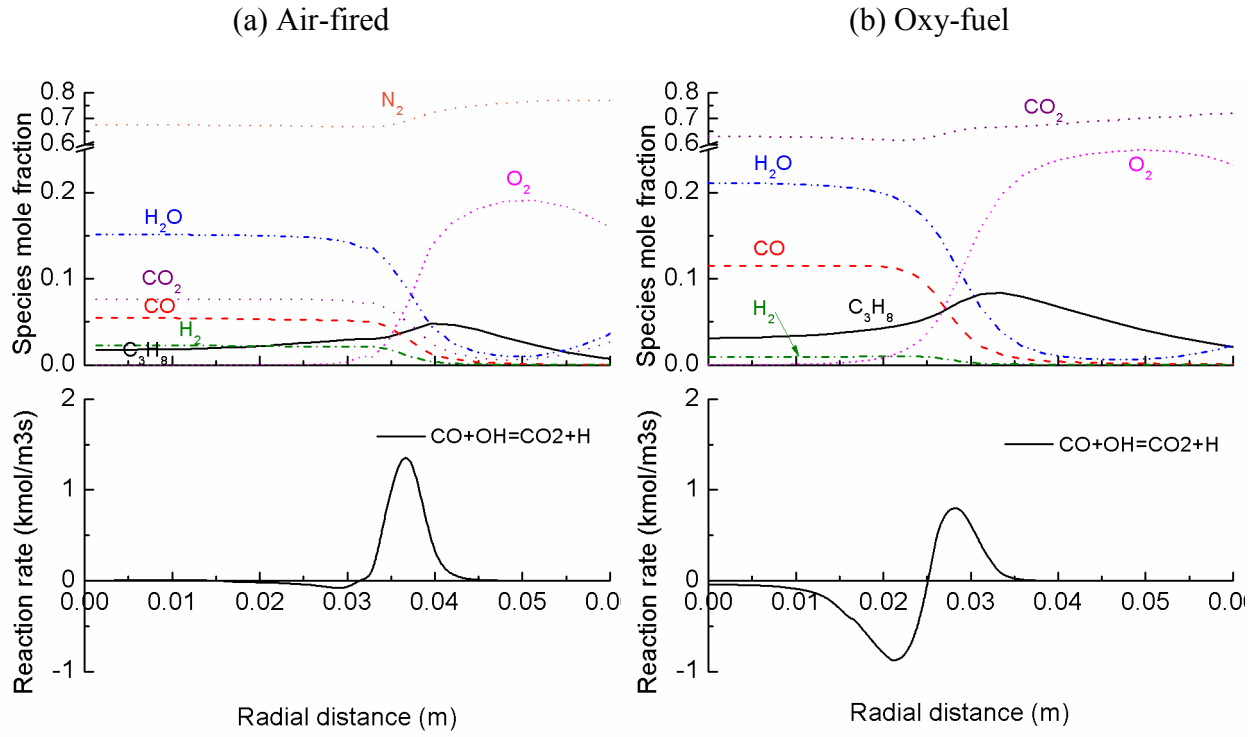
(a) Air-fired   (b) Oxy-fuel

Figure 12. Comparison of the flame structures at x=0.05 m away from the burner in (a) air-fired and (b) oxy-fuel swirling flow diffusion flames. Figures show the predicted profiles of species mole fractions and rates of the reaction $OH+CO \rightleftharpoons H+CO_2$. Results are obtained using the WDmult reaction mechanism.

References

Andersen, J., Rasmussen, C.L., Giselsson, T. and Glarborg, P. (2009). Global Combustion Mechanisms for Use in CFD Modeling under Oxy-Fuel Conditions. *Energy & Fuels* 23, 1379-1389.

Andersson, K., Johansson, R., Johnsson, F. and Leckner, B. (2008). Radiation Intensity of Propane-Fired Oxy-Fuel Flames: Implications for Soot Formation. *Energy & Fuels* 22, 1535-1541.

Andersson, K. and Johnsson, F. (2007). Flame and radiation characteristics of gas-fired O2/CO2 combustion. *Fuel* 86, 656-668.

ANSYS (2009). *ANSYS FLUENT 12.0 Theory Guide*.

Beer, J.M. and Chigier, N.A. (1983). *Combustion aerodynamics*. Malabar, Fla.: Krieger.

Buhre, B.J.P., Elliott, L.K., Sheng, C.D., Gupta, R.P. and Wall, T.F. (2005). Oxy-fuel combustion technology for coal-fired power generation. *Progress in Energy and Combustion Science* 31, 283-307.

Chen, L. and Ghoniem, A.F. (2012). Simulation of Oxy-Coal Combustion in a 100 kWth Test Facility Using RANS and LES: A Validation Study. *Energy & Fuels* 26, 4783-4798.

Chen, L., Yong, S.Z. and Ghoniem, A.F. (2012). Oxy-fuel combustion of pulverized coal: Characterization, fundamentals, stabilization and CFD modeling. *Progress in Energy and Combustion Science* 38, 156-214.

Chui, E.H. and Raithby, G.D. (1993). COMPUTATION OF RADIANT HEAT TRANSFER ON A NONORTHOGONAL MESH USING THE FINITE-VOLUME METHOD. *Numerical Heat Transfer, Part B: Fundamentals* 23, 269-288.

Dryer, F.L. and Glassman, I. (1973). High-temperature oxidation of CO and CH4. *Symposium (International) on Combustion* 14, 987-1003.

Glarborg, P. and Bentzen, L.L.B. (2008). Chemical Effects of a High CO2 Concentration in Oxy-Fuel Combustion of Methane. *Energy & Fuels* 22, 291-296.

Gregory P. Smith, David M. Golden, Michael Frenklach, Nigel W. Moriarty, Boris Eiteneer, Mikhail Goldenberg, C. Thomas Bowman, Ronald K. Hanson, Soonho Song, William C. Gardiner, J., Vitali V. Lissianski and Qin, Z. (2009) *GRI-Mech 3.0.* Retrieved from http://www.me.berkeley.edu/gri_mech/

Hjartstam, S., Andersson, K., Johnsson, F. and Leckner, B. (2009). Combustion characteristics of lignite-fired oxy-fuel flames. *Fuel* 88, 2216-2224.

Hjärtstam, S., Johansson, R., Andersson, K. and Johnsson, F. (2012). Computational Fluid Dynamics Modeling of Oxy-Fuel Flames: The Role of Soot and Gas Radiation. *Energy & Fuels* 26, 2786-2797.

Hjärtstam, S., Normann, F., Andersson, K. and Johnsson, F. (2012). Oxy-Fuel Combustion Modeling: Performance of Global Reaction Mechanisms. *Industrial & Engineering Chemistry Research* 51, 10327-10337.

Hottel, H.C. and Sarofim, A.F. (1967). *Radiative transfer*. New York,: McGraw-Hill.

Johansson, R., Andersson, K., Leckner, B. and Thunman, H. (2010). Models for gaseous radiative heat transfer applied to oxy-fuel conditions in boilers. *International Journal of Heat and Mass Transfer* 53, 220-230.

Jones, W.P. and Lindstedt, R.P. (1988). Global reaction schemes for hydrocarbon combustion. *Combustion and Flame* 73, 233-249.

Khan, I.M. and Greeves, G. (1974). A method for calculating the formation and combustion of soot in diesel engines In N. H. Afgan and J. M. Beer (eds.) *Heat Transfer in Flames*. Washington: Scripta Book Co.

Liu, F., Guo, H. and Smallwood, G.J. (2003). The chemical effect of CO2 replacement of N2 in air on the burning velocity of CH4 and H2 premixed flames. *Combustion and Flame* 133, 495-497.

Liu, F., Guo, H., Smallwood, G.J. and Gülder, Ö.L. (2001). The chemical effects of carbon dioxide as an additive in an ethylene diffusion flame: implications for soot and NOx formation. *Combustion and Flame* 125, 778-787.

Liu, H., Zailani, R. and Gibbs, B.M. (2005). Pulverized coal combustion in air and in O2/CO2 mixtures with NOx recycle. *Fuel* 84, 2109-2115.

Magnussen, B.F. (1981). On the Structure of Turbulence and a Generalized Eddy Dissipation Concept for Chemical Reaction in Turbulent Flow *19th AIAA Aerospace Science Meeting*. St.Louis, Missouri.

Magnussen, B.F. and Hjertager, B.H. (1977). On mathematical modeling of turbulent combustion with special emphasis on soot formation and combustion. *Symposium (International) on Combustion* 16, 719-729.

Masri, A.R., Dibble, R.W. and Barlow, R.S. (1992). Chemical kinetic effects in nonpremixed flames of H2/CO2 fuel. *Combustion and Flame* 91, 285-309.

Menter, F.R. (1994). Two-Equation Eddy-Viscosity Turbulence Models for Engineering Applications. *AIAA Journal* 32, 1598-1605.

Okazaki, K. and Ando, T. (1997). NOx reduction mechanism in coal combustion with recycled CO2. *Energy* 22, 207-215.

Raithby, G.D. and Chui, E.H. (1990). A Finite-Volume Method for Predicting a Radiant Heat Transfer in Enclosures With Participating Media. *Journal of heat transfer* 112, 415-423.

Rehfeldt, S., Kuhr, C., Ehmann, M., Bergins, C., Scheffknecht, G., Maier, J. and Wu, S. (2009). Basic experiments and CFD calculations of air and oxyfuel firing of lignite and bituminous coals in 0.5 and 1 MW scale combustion test facilities *The 34th International Technical Conference on Clean Coal and Fuel Systems*. Clearwater, FL.

Singer, S.L., Chen, L. and Ghoniem, A.F. (2012). The Influence of Gasification Reactions on Char Consumption under Oxy-Combustion Conditions: Effects of Particle Trajectory and Conversion. *Proceedings of the Combustion Institute* DOI:10.1016/j.proci.2012.07.042.

Spalding, D.B. (1971). Mixing and chemical reaction in steady confined turbulent flames. *Symposium (International) on Combustion* 13, 649-657.

Toftegaard, M.B., Brix, J., Jensen, P.A., Glarborg, P. and Jensen, A.D. (2010). Oxy-fuel combustion of solid fuels. *Progress in Energy and Combustion Science* 36, 581-625.

Wall, T., Liu, Y., Spero, C., Elliott, L., Khare, S., Rathnam, R., Zeenathal, F., Moghtaderi, B., Buhre, B., Sheng, C., Gupta, R., Yamada, T., Makino, K. and Yu, J. (2009). An overview on oxyfuel coal combustion--State of the art research and technology development. *Chemical Engineering Research and Design* 87, 1003-1016.

Westbrook, C.K. and Dryer, F.L. (1984). Chemical kinetic modeling of hydrocarbon combustion. *Progress in Energy and Combustion Science* 10, 1-57.

Westbrook, C.K. and Dryer, F.L. (1981). Simplified Reaction Mechanisms for the Oxidation of Hydrocarbon Fuels in Flames. *Combustion Science and Technology* 27, 31 - 43.

Woycenko, D., van de Kamp, W. and Roberts, P. (1995). Combustion of pulverized coal in a mixture of oxygen and recycled flue gas. Report No. IFRF Doc F98/Y/4.

Zheng, L. (2011). *Oxy-fuel combustion for power generation and carbon dioxide (CO$_2$) capture*. Philadelphia: Woodhead Publishing Limited.

Zheng, L. and Furimsky, E. (2003). Assessment of coal combustion in O2+CO2 by equilibrium calculations. *Fuel Processing Technology* 81, 23-34.

Zhu, D.L., Egolfopoulos, F.N. and Law, C.K. (1989). Experimental and numerical determination of laminar flame speeds of methane/(Ar, N2, CO2)-air mixtures as function of stoichiometry, pressure, and flame temperature. *Symposium (International) on Combustion* 22, 1537-1545.